Geometric Approximations for an Eight Node Thick Shell Element

Alan K. Minga*
University of Alabama
Tuscaloosa, Alabama

Abstract

Honeycomb sandwich shell analysis is difficult because an analytical solution can only be obtained for shells of very specific geometry (i.e. shells of revolution) under specific loading conditions. This paper presents the results of a portion of the author's thesis research in finite element analysis of doubly curved honeycomb shells. The focus of this paper is the development of the approximate element geometry used in the shell element. This geometry is computed internally by the code through a reasonable choice of the shell element surface coordinate system. For thick shell element analysis a reduced integration technique is used to suppress shear locking. The actual shell geometry is represented accurately by the approximations of this element. Test cases with known exact solutions proved the validity of the element in predicting the displacements of honeycomb plates and shells. The accuracy of the element in predicting stresses in the shell is comparable to other finite element codes.

Introduction

Shell structures are an important part of all engineering disciplines. Because of the presence of curvature of its surface, the bending and extension of a shell are inherently coupled. This geometric coupling results in part of the bending (out of plane loads) being carried by loads in the plane of the shell surface.

The finite element method makes the stress and displacement analysis of shells tractable. Shells can be modeled using a four node flat plate element. However, to accurately model the geometry of a curved surface, a minimum of eight nodes (four corner and four midside nodes) and an element of parabolic order is needed. The element described herein is an eight node element (Figure 1) that includes the effects of shear deformation for accurate modeling of honeycomb composites. J. N. Reddy [1] has developed a shear deformable shell element for laminated composite materials. The laminate materials were considered to be orthotropic only. Honeycomb was not considered and the geometry of his element was not computed internally but was analytically defined. As a result, his development was limited to simple geometries (cylindrical and spherical shells) which can be expressed as analytical functions. The goal of this study is to develop an eight node shell element for the analysis of orthotropic honeycomb shells of arbitrary curvature. This element is coded in FORTRAN such that the code would provide the capability to modify the output to suit specialized needs. While this capability is inherent in the commercial code NASTRAN [2] a user must use a unique language to implement it.

The element developed here includes reduced integration methods to make it applicable to thick as well as thin shells. The element is based upon the shell element developed by Reddy and includes approximations to geometry so that shells of arbitrary curvature may be represented. The topic of this paper is the geometric approximations made in the development of the eight node shell element. In this element is assumed that the isoparametric coordinates of the parent element form a set of orthogonal surface coordinates within the domain of that element. This allows the Cartesian coordinates to be expressed as functions of the surface coordinates, simplifying the computation of the element surface metrics and the quantities that they affect, distributed loads and displacement transformation.

Element Development

Shell Geometry

The development of the shell element starts with the basic definition of its geometry. The geometry, defined by the radii of curvature and the metric coefficients, appears in the equations for the shell stiffness, distributed loads and coordinate transformations.

To begin the development of the element, the isoparametric coordinates ξ and η of the parent element are assumed to be an orthogonal coordinate system on the surface of the element (see Figure 1).

---

* Graduate Student, Student Member of AIAA

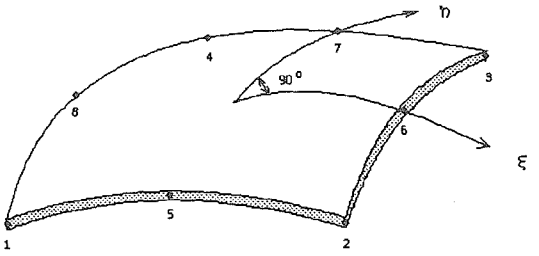

Figure 1
Node Numbering and Surface Coordinates

With this assumption the fundamental magnitudes of the surface are greatly simplified. An element of area on the surface is given by an area bordered by the ξ and η coordinate lines. If the surface coordinates are orthogonal the area of this element is given by:

$$dA_e = \alpha_1 \alpha_2 d\xi d\eta \tag{1}$$

The Cartesian coordinates may be written in terms of the coordinates of the parent element:

$$x(\xi,\eta) = \sum_{i=1}^{8} \Psi_i(\xi,\eta) x_i \tag{2}$$

$$y(\xi,\eta) = \sum_{i=1}^{8} \Psi_i(\xi,\eta) y_i \tag{3}$$

$$z(\xi,\eta) = \sum_{i=1}^{8} \Psi_i(\xi,\eta) z_i \tag{4}$$

Now recall that the fundamental magnitudes of the surface are given by:

$$\alpha_1^2 = \left(\frac{\partial x}{\partial \xi}\right)^2 + \left(\frac{\partial y}{\partial \xi}\right)^2 + \left(\frac{\partial z}{\partial \xi}\right)^2 \tag{5}$$

$$\alpha_2^2 = \left(\frac{\partial x}{\partial \eta}\right)^2 + \left(\frac{\partial y}{\partial \eta}\right)^2 + \left(\frac{\partial z}{\partial \eta}\right)^2 \tag{6}$$

With the approximate form of the shell geometry (equations 2, 3, and 4) the fundamental magnitudes may be represented in terms of the derivatives of the shape functions [3] of the element and the coordinates of the nodes of the element. These relations may be used to find the fundamental magnitudes of the surface (equations 5 and 6) for the approximate geometry of the surface.

The radii of curvature also must be computed from the approximate geometry of the surface. The radii of curvature is a vector quantity having a magnitude and a direction. The direction is given by the unit normal to the surface, while the magnitudes of the curvatures may be found from the curvature tensor β_{ab}. The curvature tensor is formed by taking the product of the appropriate component of the unit normal to the surface and the magnitude of the curvature in that direction:

$$\beta_{11} = \frac{\partial^2 x}{\partial \xi^2} \hat{n}_x + \frac{\partial^2 y}{\partial \xi^2} \hat{n}_y + \frac{\partial^2 z}{\partial \xi^2} \hat{n}_z \tag{7}$$

$$\beta_{12} = \frac{\partial^2 x}{\partial \xi \partial \eta} \hat{n}_x + \frac{\partial^2 y}{\partial \xi \partial \eta} \hat{n}_y + \frac{\partial^2 z}{\partial \xi \partial \eta} \hat{n}_z \tag{8}$$

$$\beta_{22} = \frac{\partial^2 x}{\partial \eta^2} \hat{n}_x + \frac{\partial^2 y}{\partial \eta^2} \hat{n}_y + \frac{\partial^2 z}{\partial \eta^2} \hat{n}_z \tag{9}$$

Note that the magnitudes of the curvature tensor are second derivatives of the coordinate functions of ξ and η. This is important as it dictates the minimum order of the shape functions that must be used to approximate the geometry of the element. Because the magnitudes of the curvature tensor involve second derivatives of the shape functions a bi-quadratic function must be used for all eight interpolation functions.

Once the components of the curvature tensor have been determined, the principal curvatures may be found from the roots of equation 10:

$$\begin{vmatrix} \alpha_{11} - \kappa\beta_{11} & \beta_{12} \\ \beta_{21} & \alpha_{22} - \kappa\beta_{22} \end{vmatrix} = 0 \tag{10}$$

The terms α_{12} have been dropped from equation 10 because they are zero for an orthogonal coordinate system. Equation 10 represents the curvatures along lines of principal curvature (the maximum and minimum curvatures of the surface). If the surface coordinate system is orthogonal then

coordinate lines on the surface (denoted by ξ = const and η = const) correspond to the lines of principal curvatures and the principal curvatures (equation 10) become curvatures in the directions of the coordinate lines. The radii of curvature may then be found by taking the inverse of the curvatures:

$$R_1 = \frac{1}{\kappa_1} \tag{11}$$

$$R_2 = \frac{1}{\kappa_2}. \tag{12}$$

This is only valid when the surface coordinates are orthogonal.

For computational purposes, the stiffness matrix was expressed in terms of the curvatures. If an element is singly curved or completely flat, the radii of curvature become infinite. It is completely permissible to make the substitution of radii of curvature (equations 11 and 12) as long as careful attention is paid to the signs of curvature and radii of curvature. Curvature is positive when the curve or surface is concave up. On the other hand, the radii of curvature is considered positive in the direction of the outward normal. Therefore, a positive radius of curvature corresponds to a negative surface curvature.

Element Integration

The principle of virtual work is used to develop the stiffness matrix for the shell element. Because the virtual work statement results in equilibrium equations for the element, this principle assures that the final element will be in static equilibrium for all independent virtual displacements.

The virtual work expression may be used to derive the total equilibrium statement for an element; as well as the entire structure. Since the element is derived from the part of the virtual work expression corresponding to the virtual strain energy, it will serve as the beginning of this derivation. For a plate or shell, the virtual work of the internal forces takes the same form:

$$\delta W = \int_{A_e} \left\{ \delta\varepsilon^{0t}\mathbb{N} + \delta\kappa^{t}\mathbb{M} + \delta\varepsilon^{st}\mathbb{Q} \right\} dA_e \tag{13}$$

Since equation 13 contains the transverse shear terms, it is applicable to honeycomb plates and shells as well as thick shells in general.

An element of area on the surface of a shell bounded by the ξ and η coordinates can be written in terms of the magnitudes of two vectors lying in the surface in the ξ and η coordinates (equation 1).

Which may be substituted into the equation 13 for the differential area of the element:

$$\delta W = \int_{-1}^{1}\int_{-1}^{1} \left\{ \delta\varepsilon^{0t}\mathbb{N} + \delta\kappa^{t}\mathbb{M} + \delta\varepsilon^{st}\mathbb{Q} \right\} \alpha_1\alpha_2 d\xi d\eta \tag{14}$$

Note that equation 14 is still valid for a plate element as the components of the surface vectors α_1 and α_2 are defined for any surface.

The integration of the stiffness is now taken over the region of the parent isoparametric element. The magnitudes of the surface metrics α_1 and α_2 also take on the task of mapping the original curved element onto the parent element. The isoparametric element coordinates have been chosen to coincide with the principal shell coordinates so that all material properties and displacements may be referenced to the isoparametric element coordinates. Later, this will be used to derive a transformation from the element coordinate system to the global Cartesian coordinate system.

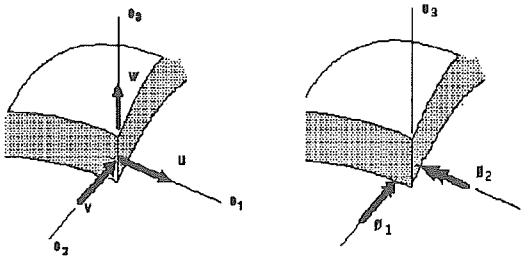

Translational Rotational

Figure 2
Element Translational and Rotational Degrees of Freedom

It can be shown that by making the statement of virtual work with respect to all independent virtual displacements (the nodal displacement vector) equal to zero, equilibrium of the element is enforced. The virtual

displacement vector is completely arbitrary. Therefore, the internal forces and the externally applied forces must be equal and opposite. The internal forces are the product of the stiffness matrix and the nodal displacement vector implying that the stiffness matrix for an element in the shell coordinates for that element is given by the integral term of equation 14. Restated, the form of the stiffness matrix is an integral equation over the domain of the parent isoparametric element where the integrand is given by equation 14:

$$[k'] = [\partial\psi]^t [S_d]^t [ABD][S_d][\partial\psi] \tag{15}$$

Numerical Integration

The integral form for the stiffness matrix requires that equation 14 be integrated over an arbitrary domain. This integration cannot be carried out analytically for a general element so a numerical integration method must be used to compute the elements of the stiffness matrix. In this analysis Gauss integration was used to integrate the equations to determine the element stiffness.

The number of Gauss points is important as it takes a minimum order of integration to represent a polynomial of a given order. For the parabolic element used to represent the shell in this analysis it has been suggested [Reddy[5] and Hughes[6] and his associates] that a 3X3 Gauss rule be used to integrate the element bending terms of the stiffness matrix. Note that this 3X3 integration rule is applied only to the bending terms in the stiffness matrix. If a 3X3 Gauss integration rule is used for the transverse shear terms the element becomes progressively stiffer as the thickness is reduced and the "shear locking" phenomena occurs [5, 6, 7, 8, and 9].

Several arguments may be presented to explain shear locking. The first of these arguments considers a beam element that may be extended to a shell [6]. A structure divided into N beam elements contains 2N degrees of freedom. The introduction of the transverse shear strain terms to the statement of virtual work imposes a constraint on the element for every Gauss point used. If a two point Gauss rule is used, two constraints are placed on the element and it "locks" because the number of constraints equals the number of degrees of freedom. A one point integration rule introduces only one constraint per element so that no locking occurs. Extending this argument to a shell element, a 2X2 Gauss integration rule is used to prevent shear locking [9, 5, 7, and 10].

In addition, consider that the contribution of the bending terms to the strain energy is proportional to h^3 while the transverse shear and inplane terms are proportional to h. As the thickness of the shell approaches zero, the strain energy becomes dominated by the shear and inplane terms. Reduced integration relieves the effects of this anomaly by introducing a singularity in the shear terms of the stiffness matrix [6]. Using a 3X3 Gauss integration rule on the inplane terms is applicable for a plate element but causes an excess amount of strain energy to be stored in membrane forces for a shell unless a 2X2 rule is used to integrate the inplane stiffness terms [7]. Note that the element cannot assume any hourglass modes because hourglassing in one element is restrained by the presence of its neighbors.

The final argument for reduced integration[11] is the division of strains volumetric, devatoric, and shear components. The devatoric strains may be integrated using a full Gauss rule. The volumetric strains must be integrated using a reduced rule because of the incompressibility of most materials. The authors also suggest a reduced rule for the transverse strains.

Consistent Load Vector

The applied loads are considered by returning to the statement of virtual work. It is not sufficient that the equivalent nodal point loads conform to the conditions of static equilibrium but they must also do the same amount of work on the body as the distributed loads that they replace. Only two types of loads are considered to act on the shell in this analysis: concentrated forces and moments acting directly on the nodes of the shell, and pressure loads distributed across the shell surface.

Normal Pressures

The code developed for this paper was intended primarily for the analysis of aircraft structures where the primary cause of distributed pressure loads is the aerodynamic forces on the vehicle. Such loads only act normal to the vehicle surface. Hence, only normal pressures were considered in the analysis.

The pressure loads acting over the surface of a typical aircraft shell structure such as a missile nose cone or an aircraft radome is usually a complicated function of the position on the shell. However, if the

pressure is considered only over the domain of one element, it may be represented closely by a bilinear pressure distribution which is defined by specifying the pressures at each of the four corner gridpoints of the element. A linear interpolation in terms of the surface coordinates ξ and η is then applied to approximate the variation in pressure across the surface:

$$P(\xi,\eta) = \sum_{i=1}^{4} P_i (1+\xi_i \xi)(1+\eta_i \eta) \tag{16}$$

In this analysis, it is necessary to express the pressure loads in terms of loads applied directly to the nodes of the element. To derive the nodal load contributions from a given pressure load, it is necessary to use the statement of virtual work.

For a pressure load the virtual work is the product of the pressure and the normal displacement integrated across the region of an element:

$$\delta W = - \int_{A_e} P(\xi,\eta)\delta w(\xi,\eta) dA_e \tag{17}$$

Hence, if equation 1 is substituted into equation 17 the virtual work statement for the applied pressure loads can be written in the same form as the element stiffness, as an integral over the parent isoparametric element. The integral portion of this equation will be the force terms conjugate to the virtual displacements $\{\delta w\}$. The implications of this statement are quite important. Only the force terms conjugate to the virtual normal displacements are the forces applied normal to the shell surface. Therefore, if only first order deformation terms are considered, only normal forces can be produced by a normal pressure. These forces at node i may be computed by integrating the pressure weighted by the appropriate shape function over the domain of a parent element:

$$F_i = \int_{-1}^{1}\int_{-1}^{1} P(\xi,\eta)\psi_i \alpha_1 \alpha_2 d\xi d\eta \tag{18}$$

Equation 18 was evaluated analytically and coded in terms of the pressures at the corner nodes for an arbitrary shell element. For this paper the nodal forces were evaluated by numerically integrating the pressures over the element. A 3X3 Gauss rule was used to integrate the pressures and obtain the nodal point forces.

Element Performance

The shell element described herein was developed to model shells of arbitrary curvature. However, since no exact solutions exist for shells of arbitrary curvature performance of this element must be evaluated on specific geometries where exact solutions exist. Table 1 shows the test cases used to evaluate the accuracy and performance of the shell element.

These cases represent all combinations of geometry for which analytical solutions exist. For all of these cases the finite element code was used to compute the defining geometric quantities of the shell (metric coefficients and radii of curvature). The deflections used for comparison in cases 1, 2 and 4 was the normal deflection at the center of the center of the model. Stress and moment resultant errors were compared instead of actual lamina stresses because the resultant give an over all picture of stress in the elements. The stress resultant are defined for an element while the stress is defined for each lamina. NASTRAN models were assembled using the QUAD8 element as it is the closest element to the one presented in this paper. All stress resultant were measured near the supported edge as a worst case analysis.

Flat Plate Solutions

The first test case for element performance was a simply supported orthotropic sandwich plate under a

Table 1
Shell Element Analysis Cases

Case	Benchmark	Quantity Compared
Plate	Exact Solution NASTRAN	Deflection Stresses
Clamped Orthotropic Cylinder	Exact Solution NASTRAN Reddy's Shell Element	Deflection
Clamped Sandwich Cylinder	NASTRAN	Stresses
Sphere	Exact Solution	Deflection

uniform load of 10 psi. Material properties (Table 2) represent those of a typical aircraft radome with glass fiber face sheets.

Two core thicknesses were used in the analysis 0.1 in and 0.5 in, corresponding to thick and thin shells, respectively.

Because of biaxial symmetry only a quarter of the plate was modeled using appropriate boundary conditions to enforce the effects of biaxial symmetry. A 4 X 4 mesh of shell elements was used to model the quarter plate. Figure 4 shows the mesh of elements and boundary conditions used for the paper element and the NASTRAN model.

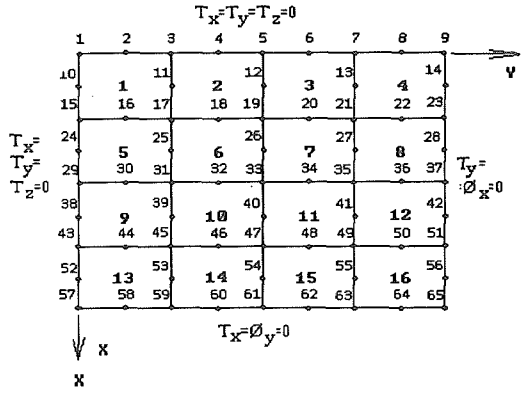

Figure 3
Flat Plate Element and Node Numbering

Predictions of the center deflection (Table 3) of the plate agree well with NASTRAN and the exact solution based on a Fourier Series [13].

Note that the finite element solutions are more flexible than the exact solution contrary to what is expected in a descretized displacement model. While no exact reason for this is known it is believed that this is due to the underprediction of the element area by the finite element solutions. In spite of this anomaly, agreement with the exact solution is excellent (maximum error 2.2%). These data also indicate that the element does not "lock" as the thickness is reduced.

The stress resultant predicted by the finite element solutions do not agree well with those predicted by the exact solution. The element stress resultant do however, agree well with those predicted by NASTRAN. Note in Figures 5 to 8 the difference is small for the thin plate case. In these plots the element appears to have a large error for Mx in the thin plate case. This is misleading as the numerical values of the moment resultant are small for this case causing a rather small numerical error to appear as a large percent error. Note that the profile shown in the figures was taken 1.25 inches from the supported edge of the plate. It is believed that these factors contributed to the difference in stress resultant. The latter hypothesis is supported by the fact that error in resultant decreases as the center of the plate is approached. The inplane stress resultant were correctly predicted as zero by both finite element solutions.

Table 2
Sandwich Material Properties

Face Sheets	Core
$E_x = 3.7 \times 10^6$ psi	$E_x = 100$ psi
$E_y = 3.2 \times 10^6$ psi	$E_y = 100$ psi
$\nu_{xy} = .11$	$\nu_{xy} = .3$
$G_{xy} = 5.1 \times 10^5$ psi	$G_{xy} = 100$ psi
thickness = 0.02 in	$G_{1Z} = 1.4 \times 10^4$ psi
	$G_{2Z} = 5.0 \times 10^3$ psi

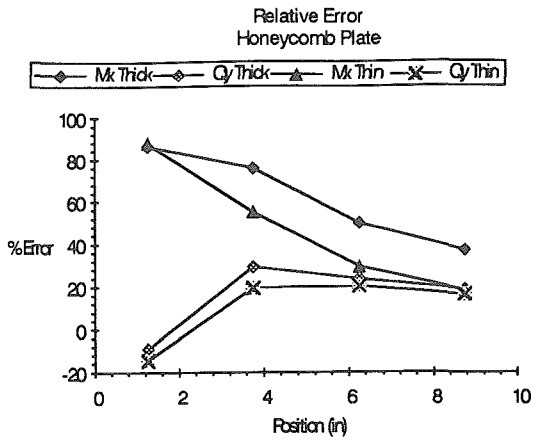

Figure 4
Honeycomb Plate Stress Error
Relative to Exact Solution

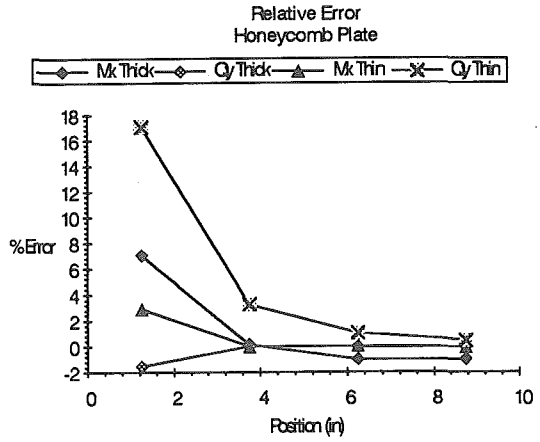

Figure 5
Honeycomb Plate Stress Error
Relative to NASTRAN

Cylindrical Shell Solutions

Two test cases were used to verify the element's accuracy on cylindrical shell problems. Both test cases used identical geometry, a circular cylinder (R=10 in, length = 20 in) clamped at both ends and pressurized to $6.4/\pi$ psi. As in the Test Case 1 biaxial symmetry permitted $\frac{1}{8}$ of the cylinder to be used as a model. A 4X4 mesh of elements identical in numbering to those used for the flat plate analysis was used to model both cylinders.

The first cylinder test case corresponds to an exact solution presented by Reddy [1] for an orthotropic non-sandwich shell. Material properties for this test case are presented in Table 4.

Table 4
Orthotropic Shell Material Properties

E_1	=	7.50×10^6
E_2	=	2.00×10^6
$G_{12} = G_{13} = G_{23}$	=	1.25×10^6
$\nu_{12} = \nu_{21}$	=	0.2

This case was used to verify element displacements for a cylindrical shell as an exact solutions exist for was readily available. Table 5 shows the normal displacement of the cylinder at L/2.

Table 5
Center Deflections of an Orthotropic Cylinder

Analysis	Center Deflection (in)
Reddy (Exact)	3.6700×10^{-4}
Reddy (linear elements)	3.7540×10^{-4}
Reddy (quadratic elements)	3.7270×10^{-4}
NASTRAN	3.6858×10^{-4}
This Element	3.6772×10^{-4}

For this test case the performance of the element developed here is even better than that of the element from which it was derived (Reddy's quadratic shell element). The element slightly overpredicts the curvature of the surface. This apparent error in the geometry results in better displacement prediction due to the increased apparent stiffness.

The second cylindrical test case was introduced to verify the accuracy of the stresses predicted by the element for honeycomb shells. Material properties used were those in Table 2. No exact solution was available

Table 3
Flat Plate Center Deflections

Solution Method	$t_c = 0.1$	$t_c = 0.5$
NASTRAN	19.139	1.1077
Exact Solution	19.275	1.0902
This Paper	19.334	1.1151

so results were compared against NASTRAN. Figure 7 shows the error in primary inplane, bending and transverse stress resultant plotted along the length of the shell for the thick (t_c = 0.5) and thin shell (t_c = 0.1) cases. Agreement with NASTRAN is excellent for both cases proving that the element does not lock under thin shell conditions. Once again some of the stress resultant are small causing their percentage error to appear large. This agreement also validates the use of reduced integration on the inplane stiffness. In all cases the behavior of the stress resultant at the boundaries appeared to be correct, although it can be deduced from the plate analysis that the resultant are probably overpredicted in this case also.

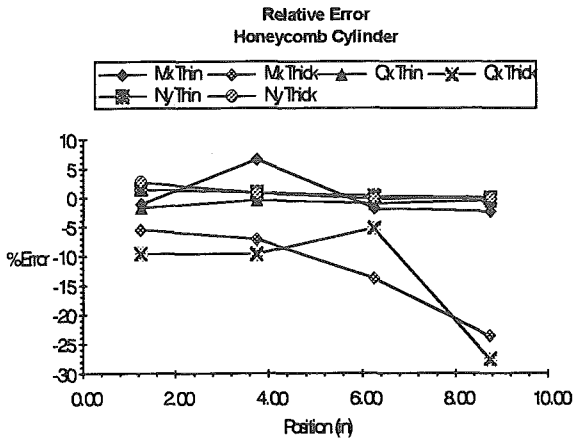

Figure 6
Cylindrical Honeycomb Shell Error Comparison
Realtive to NASTRAN

Spherical Shell Solutions

The spherical shell represents a double curved shell for which an exact solution exist. The shell presented here corresponds to a simply supported spherical vault. Shell dimensions and material properties are presented in Table 6.

Center deflections of the shell (Table 7) compare well to both those predicted by the exact solution and NASTRAN for the 2 X 2 mesh of elements used. No stresses are predicted by the exact solution so they were not compared in this case. It is felt that the two sandwich test cases sufficiently prove the accuracy of the element in computing stresses.

Table 6
Spherical Shell Properties

$R_1 = R_2 = 96$ in
$a = b = 36$ in
shell thickness = 3.6 in
Lamination Sequence $0^0/90^0/90^0/0^0$
$E_1 = 25 \times 10^6$
$E_2 = 1 \times 10^6$
$\nu_{12} = .25$
$G_{12} = G_{23} = G_{13} = 0.5 \times 10^6$

Table 7
Center Deflections of a Spherical Vault

Reddy	1.468×10^{-3}
NASTRAN	1.489×10^{-3}
This Element	1.501×10^{-3}

Conclusions

A new finite element has been developed for the analysis of laminated composite materials, including honeycomb sandwich shells. The element features internal geometry processing and provides stress and displacement predictions for all combinations of single, double and no curvature of the element.

From the research done in this paper conclusions can be made about performance of the element:

1. Reduced integration of the transverse shear terms eliminates the effects of "shear locking".

2. Reduced integration of the inplane stiffness terms is valid as no type of hourglass instability was encountered. This step reduced the computational expense of the element.

3. Displacement predictions of the element are excellent, with maximum error (2.2%) occurring for flat plate analysis.

4. Internal computation of the radii of curvature can be accomplished if the proper order of interpolation functions are chosen. The small errors in predicting the radii of curvature resulted in increased accuracy due to the additional stiffness they created.

5. Stresses predicted by the element are high in comparison to analytical solutions; however, they are no worse than other finite element methods. The element errs on the conservative side making it suitable for design purposes.

The element developed herein is simple enough that no Supercomputer is required to run the code. Run times on an IBM 3090 are less than those of NASTRAN on a CRAY X/MP 24. The code is written in FORTRAN and may be modified easily for future use. All of the goals of this study were met.

Acknowledgments

The author wishes to express his thanks to Dr. George E. Weeks without whose help and guidance this research would have not been possible.

References

1. Reddy, J. N., *Energy and Variational Methods in Applied Mechanics.* John Wiley and Sons, New York, NY, 1984.

2. MacNeal, Richard H., "A Simple Quadrilateral Shell Element", *Computers and Structures*, Vol. 8, 1978, pp. 175 - 183.

3. Ahmad, Sohrabuddin; Irons, Bruce M.; and Zienkiewicz, O. C., "Analysis of Thick and Thin Shell Structures by Curved Finite Elements", *International Journal for Numerical Methods in Engineering*, Vol. 2, 1970, pp. 419 - 451.

4. Minga, A. K. *Development of a Shear Deformable Element for Finite Element Analysis of Double Curved Honeycomb Shells.* The University of Alabama, Tuscaloosa, AL 1989.

5. Reddy, J. N., "Bending of Laminated Anisotropic Shells by a Shear Deformable Finite Element", *Fiber Science and Technology*, Vol. 17, 1982, pp. 9 - 24.

6. Hughes, Thomas J. R.; Taylor, Robert L.; and Kanoknukulchai, Worsak, "A Simple and Efficient Element for Plate Bending", *International Journal for Numerical Methods in Engineering*, Vol. 11, 1977, pp. 1529 - 1543.

7. Cook, Robert D., *Concepts and Applications of Finite Element Analysis.* John Wiley and Sons, New York, NY, 1981.

8. Pugh, E. D. L.; Hinton, E.; and Zeinkiewicz, O. C., "A Study of Quadrilateral Plate Bending Elements with 'Reduced' Integration", *International Journal for Numerical Methods in Engineering*, Vol 12, 1978, pp. 1059 - 1079.

9. Reddy, J. N., "A Penalty Plate-Bending Element for the Analysis of Laminated Anisotropic Composite Plates", *International Journal for Numerical Methods in Engineering*, Vol. 15, 1980, pp. 1187-1206.

10. Reddy, J. N., *An Introduction to the Finite Element Method.* McGraw Hill, New York, NY, 1984.

11. Koh, Byeong C. and Kikuchi, Noboru, "New and Improved Hourglass Control for Bilinear and Trilinear Elements in Anisotropic Linear Elasticity", *Computer Methods in Applied Mechanics and Engineering*, Vol. 65, 1987, pp. 1-46.

12. Whitney, J. M., "Stress Analysis of Thick Laminated Composite Plates", *Journal of Composite Materials*, Vol. 6, 1972, pp. 426 - 440.

13. Platema, F. J., *Sandwich Construction.* Wiley, New York, NY, 1966.

14. Reddy, J. N., "Exact Solutions of Moderately Thick Laminated Shells", *Journal of Engineering Mechanics*, Vol. 110, 1984, pp. 794 - 809.

15. Tsai, S. W. and Hahn, H. T. *Introduction to Composite Materials.* Technomic, Lancaster, PA, 1980.

Appendix A
Shape Functions

$$\psi_i = \frac{1}{4}(1+\xi\xi_i)(1+\eta\eta_i)(\xi\xi_i+\eta\eta_i-1)$$

i=1-4

$$\psi_i = \frac{1}{2}(1+\xi\xi_i)(1-\eta^2)$$

i=6,8

$$\psi_i = \frac{1}{2}(1-\xi^2)(1-\eta\eta_i)$$

i=5,7

Appendix B
Nomenclature

$[ABD]$ - Constitutive Relations for a Composite Material

$[\partial N]$ - Shape Functions Derivative Matrix

$[\mathbf{k}]$ - Element Stiffness Matrix in Shell Coordinates

$[\mathbf{S_d}]$ - Strain - Displacement Operator Matrix

$\{\mathbf{F}\}$ - Element Force Vector in Cartesian Coordinates

$\{\mathbf{f}\}$ - Element Force Vector in Shell Coordinates

A_e - Area of an Element

dA_e - Differential Area of an Element

E_x, E_y - Young's Modulus in Material Coordinates

G_{xy} - Inplane Shear Modulus

G_{1z}, G_{2z} - Transverse Shear Modulus

$\hat{n}$ - Unit Normal to A Surface

$\hat{n}_x, \hat{n}_y, \hat{n}_z$ - Components of the Unit Normal

P - Normal Pressure

P_i - Pressure at Node i

R_1, R_2 - Radii of Curvature in υ and η Directions

u, v, w - Continuous Displacements of A Shell

u_i, v_i, w_i - Displacements of Node i in Shell Coordinates

x, y, z - Cartesian Coordinates of A Shell

x_i, y_i, z_i - Cartesian Coordinates of the Element Nodes

$\alpha_1 \equiv \alpha_{11}$

$\alpha_{11}, \alpha_{12}, \alpha_{22}$ - Surface Metric Coefficients

$\alpha_2 \equiv \alpha_{22}$

$\beta_{11}, \beta_{12}, \beta_{22}$ - Second Fundamental Magnitudes of a Surface

$\{\Psi_i\}$ - Element Shape Functions for Node i

ϕ_1, ϕ_2 - Rotation of the Shell in the ξ,η Direction

ε^0 - Inplane Midsurface Strain Vector

ε^s - Midsurface Transverse Shear Strain Vector

κ - Surface Curvature

κ_1, κ_2 = Initial Surface Curvatures

κ - Midsurface Curvature Vector

ξ, η - Element Surface Coordinates

ξ_i, η_i - Element Surface Coordinates for Node i

δW - Virtual Work

THE INTERNATIONAL COUNCIL OF THE AERONAUTICAL SCIENCES

ICAS Officers

President: Paolo Santini, Italy

Chairman, Programme Committee: Richard H. Petersen, USA

Executive Secretary: Fred J. Sterk, The Netherlands

Honorary Treasurer: John M. Swihart, USA

Past President: Boris Laschka, Germany

H. Blenk, Germany
M. Brusseleers, Belgium
E. Campos, Spain
L.M.B.C. Campos, Portugal
G.M. Carlomagno, Italy
R.R. Dexter, USA, LM*
M.C. Dökmeci, Turkey
C. Dousset, France
J.F. Elaskar, Argentina
B. Fredriksson, Sweden
J.E. Green, United Kingdom
B.J. Habibie, Indonesia
R.V. Harris, Jr., USA
S.A. Hassan, Pakistan
M. Josifovic, Yugoslavia
D. Kontonis, Greece
S. Laine, Finland
B. Laschka, Germany
J. Lewitowicz, Poland
I.S. Macdonald, Canada
G. Madelung, Germany
O.L.P. Masefield, Switzerland
H. Nagasu, Japan
R.H. Petersen, USA
N. Rao, India
O. Rho, Korea
J. Rohács, Hungary
P. Santini, Italy
J. Shinar, Israel
J. Singer, Israel
B.M. Spee, The Netherlands
R. Staufenbiel, Germany, LM*
F.J. Sterk, The Netherlands
J.M. Swihart, USA
A.J. Vermeulen, South Africa
A.D. Young, United Kingdom
G.I. Zagainov, Russia
Zhang Yanzhong, P.R. of China

Observers:

O. Diran, Indonesia
V. Giavotto, Italy

* LM - Life Member

ICAS PROGRAMME COMMITTEE

Richard H. Petersen (Chairman), USA
Paolo Santini (ICAS President), Italy
Fred J. Sterk (Executive Secretary), The Netherlands
Yasuhiko Aihara, Japan
Vincent P. Baglio, USA
Ronald L. Bengelink, USA
Antonio Castellani, Italy
Harijono Djojodihardjo, Indonesia
Thomas F. Donohue, USA
Clement Dousset, France
Uwe Ganzer, Germany
Vittorio Giavotto, Italy
John E. Green, United Kingdom
Anders Gustafsson, Sweden
Roy V. Harris, Jr., USA
Ji Wenmei, P.R. of China
Boris Laschka, Germany
Mrs. Camille D. McCarthy, USA
Ian S. Macdonald, Canada
Jean-Pierre Marec, France
Oliver L.P. Masefield, Switzerland
Michele Onorato, Italy
Alfred Ritter, USA
Wolfgang Schmidt, Germany
Josef Shinar, Israel
Josef Singer, Israel
James M. Sinnett, USA
Ben M. Spee, The Netherlands
Egbert Torenbeek, The Netherlands
Alec D. Young, United Kingdom
German I. Zagainov, Russia
Zhang Yanzhong, P.R. of China

ICAS MEMBER ASSOCIATIONS

ARGENTINA
Universidad Nacional de Córdoba
Facultad de Ciencias Exactas, Fisicas Y Naturales
Casilla de Correo No 395,(5000) Cordóba
(Prof.Ing. J.F. Elaskar)

AUSTRALIA
The Royal Aeronautical Society
Australian Division
P.O. Box 753, Mascot, NSW 2020
(R.D. Barkla, Honorary Secretary)

BELGIUM
Royal Flemish Association of Engineers (KVIV),
Aeronautical Section
Desguinlei 214, 2018 Antwerpen
(P. de Swert, President)

BRAZIL
Instituto Brasileiro de Aeronautica
Ave Marechal Camara
233-S/1203,20,000
Rio de Janeiro GB

CANADA
Canadian Aeronautics and Space Institute (CASI)
130, Slater Street, Suite 818
Ottawa, Ontario K1P 6E2
(A.J.S. Timmins, Executive Director)

CHINA (People's Republic of)
Chinese Society of Aeronautics and
Astronautics (CSAA)
No. 9 Xiaoguandongli, Anwai,
Chaoyang District, Beijing 100029
(Prof. Zhang Yanzhong, Secretary General)

CZECHOSLOVAKIA
Czechoslovak Society for Mechanics at
the Czechoslovak Academy of Sciences
Dolejskova 5, 182 00 Praha 8
(Dr. R. Dvorák, Director)

FINLAND
The Engineering Society in Finland STS
Ratavartijankatu 2, 00520 Helsinki
(M. Hirvikallio, Head of Department)

FRANCE
Association Aéronautique et Astronautique
de France (AAAF)
6, Rue Galilée, 75782 Paris Cedex 16

GERMANY
Deutsche Gesellschaft für Luft- und
Raumfahrt e.V. (DGLR)
Godesberger Allee 70, 5300 Bonn 2
(H. Schwäbisch, Secretary General)

GREECE
Greek Aeronautical Engineers Society
1, Karitsi Street, Athens, 105 61
(Dr. D. Kontonis)

HUNGARY
Scientific Society of Mechanical Engineers
P.O. Box 451, 1372 Budapest 5
(G. Friwaldszky, Executive Director)

INDIA
The Institution of Engineers (India)
8, Gokhale Road, Calcutta 700020
(Col. B.D. Varma FIE, Director General)

INDONESIA
Indonesian Aeronautical and Astronautical Institute
(ISASTI)
Gedung BPP Teknologi, Lantai 15
Jalan M.H. Thamrin 8, Jakarta
(Prof. O. Diran)

ISRAEL
Israel Society of Aeronautics and Astronautics
P.O. Box 2956, Tel-Aviv 61028
(Y. Eliraz, Chairman)

ITALY
Associazione Italiana di Aeronautica e Astronautica
(AIDAA)
Via Po 50, 00198 Rome
(Prof. P. Santini)

JAPAN
Japan Society for Aeronautical and Space Sciences
Kokukaikan-Bunkan
1-18-2 Shinbashi Minato-ku, Tokyo 105
(Prof. Y. Aihara, Director)

KOREA
The Korean Society for Aeronautical & Space
Sciences
404 Murijae Bldg. 984-1
Bangbae-3-Dong Seocho-Ku, Seoul 137-063
(Wi Hun Kang, President)

THE NETHERLANDS
Netherlands Association of Aeronautical Engineers
(NVvL)
Anthony Fokkerweg 2, 1059 CM Amsterdam
(P. Kluit, Secretary)

NEW ZEALAND
The Royal Aeronautical Society
New Zealand Division
P.O. Box 3813, Wellington
(R.J. Doggett)

PAKISTAN
The Institution of Engineers, Pakistan
I.E.P. Building, 4th Floor
177/2 Liaquat Barracks, Karachi-75530
(Dr. S.A. Hasan, Chairman Internat. Affairs)

POLAND
Polish Society of Mechanical Engineers
and Technicians
14A, Swietokrzyska, Warsaw 00-50
(Prof. J. Lewitowicz)

PORTUGAL
Minestero do Plano e da Administracao
do Território
Junta Nacional de Investigacao e Cientifica
Tecnologica
Av. D. Carlos 126-1.* e 2.*, 1200 Lisboa
(Prof. J. Mariano Gago, President)

RUMANIA
Commission d'Astronautique de l'Academie de la
Republique Socialiste de Roumanie
Str. Const. Mille No. 15, Bucuresti

RUSSIA
Central Aerohydrodynamics Institute (TsAGI)
Zhukovski, Moscow reg., 140160
(Dr. G.I. Zagainov, Director)

SOUTH AFRICA (Republic of)
AEROTEK, CSIR
P.O. Box 395, Pretoria, 0001
(Dr. A.J. Vermeulen)

SPAIN
Instituto Nacional de Técnica Aeroespacial (INTA)
Carretera de Ajalvir Km. 4
28850 Torrejón de Ardoz (Madrid)
(Prof.Dr. J.M. Quintana)

SWEDEN
Swedish Society for Aeronautics & Astronautics
(SSAA)
Swedish Space Corporation
P.O. Box 4207, 17154 Solna
(K. Lundahl, Secretary General)

SWITZERLAND
Schweizerische Vereinigung für Flugwissenschaften
ETH-Zentrum, 8092 Zürich
(G. Bridel, President)

TURKEY
Istanbul Technical University P.K. 9
Faculty of Aeronautics and Astronautics
Taskim (Maslak), Istanbul 80191
(Prof. M.C. Dökmeci)

UNITED KINGDOM
The Royal Aeronautical Society
4, Hamilton Place, London W1V 0BQ
(R.J. Kennett, Director)

USA
American Institute of Aeronautics and Astronautics
(AIAA)
370 L'Enfant Promenade, SW,
Washington DC 20024 - 2518
(Ms. M. Gerard)

YUGOSLAVIA
Yugoslav Aerospace Society
27, Marta Str. 80, 11 000 Beograd
(Prof.Dr. M. Josifović, Secretary General)

ICAS ASSOCIATE MEMBERS

BELGIUM
Von Kármán Institute for Fluid Dynamics
Chaussee de Waterloo 72
1640 Rhode-St-Genese

THE NETHERLANDS
Fokker B.V.
P.O. Box 12222
1100 AE Amsterdam Zuidoost

KLM
P.O. Box 7700
1117 ZL Schiphol

National Aerospace Laboratory NLR
P.O. Box 90502
1006 BM Amsterdam

SWEDEN
The Aeronautical Research Institute
of Sweden (FFA)
P.O. Box 11021
161 11 Bromma

The Steering Group of the Programme for the
Swedish Civil Aircraft Technology
P.O. Box 11021
161 11 Bromma

SAAB-SCANIA AB
581 88 Linköping

UNITED KINGDOM
British Aerospace plc
P.O. Box 87
Farnborough, Hampshire GU14 6YU

Rolls-Royce plc
P.O. Box 31
Derby DE2 8BJ

USA
Thomas Paine Associates
2401 Colorado Avenue
Suite 178
Santa Monica, CA 90404-3514

Rockwell International
2230 East Imperial Highway
El Segundo, CA 90245